# Risk Assessment of Geological Disasters Based on Slope Units in Town Scale
# A case study of Dazhou Town along the Yangtze River

Jie Fu[1,2,3,a], Xiuyuan Yang[2,b*], Aihong Shi[2,c], Qing Zhang[2,d], Songlin Liu[4,e]

[a]fujie@mail.cgs.gov.cn, [b*]yangxiuyuan@mail.cgs.gov.cn, [c]shiaihong@mail.cgs.gov.cn, [d]zhangqing@mail.cgs.gov.cn, [e]804807600@qq.com

[1]China University of Mining and Technology, Xuzhou, 221116, China
[2]Center for Hydrogeology and Environmental Geology Survey, CGS, Baoding, 071051, China
[3]Hebei Center for Ecological and Environmental Geology Research, Hebei GEO University, Shijiazhuang, 050031, China
[4]School of Civil Engineering, Chongqing University, Chongqing, 400045, China

**Abstract.** With the rapid urbanization, the geological disaster risk has attracted increasing attention in the safety risk of town construction. This paper proposes a six-step technical framework for geological disaster risk evaluation in town, i.e., slope unit division, rainfall condition analysis, automatic extraction of disaster-bearing bodies, hazard evaluation, quantitative evaluation of vulnerability, and risk evaluation. The migrant town along the Yangtze River, Dazhou Town in Wanzhou District of Chongqing, is selected as the study area. An improved hydrological analysis method for multi-scale division of slopes is proposed, which can be employed to extract the evaluation units for geological disaster risk. Based on the fifty-year rainfall conditions through the Gumbel distribution, the limit equilibrium method is adopted to estimate the stability and occurrence probability of slopes. Furthermore, the object-oriented approach is utilized to quickly extract information about buildings and traffic roads, etc. Finally, the hazard evaluation model and the vulnerability evaluation model are established to achieve the risk evaluation of geological disasters in towns, which are based on the slope unit and hazard source analysis, respectively. According to the risk map，$34.5\times10^3$ $m^2$ of buildings and $15.0\times10^3$ $m^2$ of roads are in the extremely high risky zone, while about $36.3\times10^3$ $m^2$ of buildings and $38.3\times10^3$ $m^2$ of roads are in the high risky zone. It is found that the results of the risk evaluation are consistent with the field observations and surveys.

**Keywords-**Risk Assessment; Town Scale; Geological disaster; Slope Unit; Disaster-bearing

## 1 Introduction

With the rapid new urbanization in China, the geological safety risks posed by urbanization construction should not be underestimated[1]. As an important area of new urbanization in China, the Three Gorges Reservoir area has become the hotspot affecting the geological safety risk of immigrant towns along the Yangtze River because of the frequent occurrence of geological

IDEE 2023, November 24-26, Zhengzhou, People's Republic of China

DOI 10.4108/eai.24-11-2023.2343450

disasters[2]–[4]. In recent years, both governments and researchers have paid more attention to the geological disaster risks in towns. In 2020, China's Ministry of Natural Resources proposed to coordinate and promote the pilot national geological disaster risk surveys. In 2021, the government of Chongqing carried out city-wide geological disaster survey and risk evaluation, providing a basis for territorial spatial planning, disaster prevention and mitigation management, etc. To mitigate the risk of geological disaster, establishing a prediction model that is capable to provide the spatial and temporal probabilities of disaster occurrence, as well as the intensity of disaster and spatial distribution of disaster-bearing bodies information, is essential but challenging[5]. Various studies have assessed the susceptibility, hazard, and vulnerability of geological disasters from regional and individual perspectives[6]–[8]. For example, several studies have used machine learning methods to evaluate susceptibility for predicting the spatial probability of geological disaster occurrence on a regional scale[9]–[15]. Several researchers have attempted to build up the hazard evaluation model by analyzing the relationship between historical disaster events and rainfall triggering factors[5], [16]–[18]. In addition, some models have been proposed for vulnerability evaluation based on statistical data, satellite image data, etc.[19]–[21]. In all the studies, the geological disaster risk analysis utilizes abundant spatial-temporal data, and various approaches including three-dimensional structure modeling, numerical modeling, statistical modeling, dynamic modeling, time series modeling, and spatial distribution modeling[22].

However, many studies on geological disaster risk evaluation have focused on a regional scale or individual scale, and there is limited research on the town scale[23]. Geological disaster risk evaluation on the town scale is an intermediate scale evaluation between regional scale and individual scale, which considers not only the pattern and threat objects of disaster from the perspective of region, but also the intensity of disaster and vulnerability of the disaster-bearing body from individual perspective. This study, taking disaster units and disaster-bearing bodies as the research objects, proposes a hazard evaluation method based on slope unit analysis and a quantitative evaluation method for the vulnerability of disaster-bearing bodies based on hazard source analysis. Finally, a set of ideas and technical method for the geological disasters risk evaluation in towns are put forward.

## 2 Materials and Methods

### 2.1 Study Area

The study area is located in Dazhou Town, Wanzhou District, Chongqing, which is a migrant town along the Yangtze River, as shown in Figure 1. The area has a northern subtropical mountain climate with abundant rainfall, with an average annual rainfall of 1,243mm. Rainfall occurs mostly in May and September, accounting for 70% of the annual precipitation. As an area highly prone to geological disasters, its terrain is strongly cut by rivers and spreads with a step-like shape, the elevation distributes in the range of 145-350m. The lithology is majorly composed by Jurassic thick, nearly horizontal sandstone sandwiching mudstone and Quaternary loose rock. According to the Seismic Parameter Zoning Map of China (GB18306-2015), the peak ground vibration acceleration (g) in this area is 0.05.

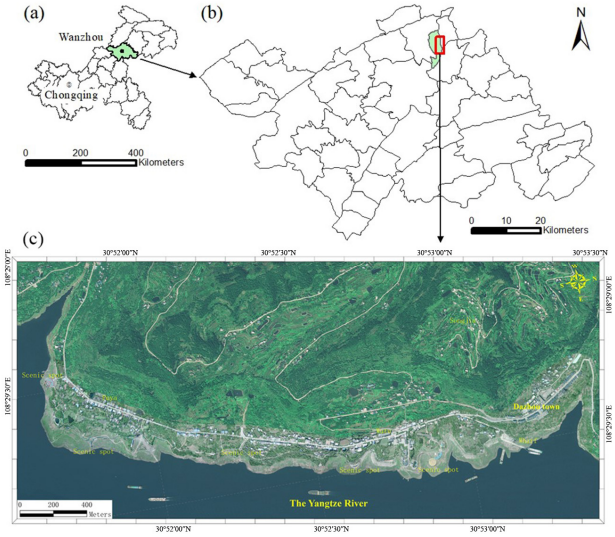


**Figure 1.** Illustration of the study area

## 2.2 Data Sources

Geological disaster risk evaluation data sources contain various elements, including temporal, spatial, macroscopic, and microscopic data. The topographic data were obtained from the digital elevation model (DEM) at a scale of 1:2000. Geological data contains stratigraphic lithology, slope structure, geotechnical parameters, surface deformation, groundwater, and other data obtained by means of survey, drilling, and trenching. The rainfall data were obtained from the National Meteorological Information Center for the last 50 years of daily rainfall at the Wanzhou site. The reservoir water level data were collected from the daily water level records of China Yangtze River Three Gorges Group Ltd. for the period 2011-2018. Land use types were deciphered by UAV aerial images. Population distribution data were collected from local government census information.

The flow chart of geological disaster risk evaluation is shown in Figure 2. The evaluation processes include two parts: the first part is the hazard evaluation based on slope unit, and the second part is the vulnerability evaluation based on hazard source analysis.

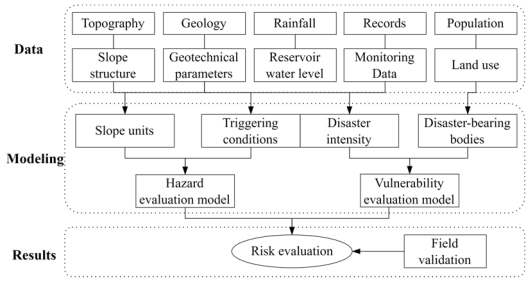


**Figure 2.** The flow chart of geological disaster risk evaluation

## 2.3 Evaluation Unit Division

The selection of evaluation units is the basis for geologic disaster risk modeling[24]. Currently, there are five common categories of evaluation units used in risk modeling, i.e., grid unit, terrain units, unique-condition units, slope units, and topographic units[25]. Among different evaluation units, the slope unit has been widely used as it can effectively reflect the physical relationship between disasters and basic terrain elements, especially in mountainous areas[26]. The traditional hydrology-based method divides slope units by extracting catchment and anti-catchment areas from the DEM through hydrological analysis[27]. The task of extracting slope units can be done directly through the hydrological analysis tool in the ArcGIS 10.2 environment. However, the approach often leads to unexpected slope units, such as illogical long strips, particularly at the area with complex topography. Therefore, it is necessary to optimize the hydrology-based method for areas with obvious terrain change. Due to the influence of geological structure and river erosion, the area along the Yangtze River has a multi-step topography, as shown in Figure 3. The topography has an obvious change of slope, which leads to different geological disasters, such as steep terrain producing collapses and gentle terrain producing landslides. To this end, we propose a modified slope segmentation method on the basis of the hydrological-based method, as shown in Figure 4. The slope segmentation method, as compared to the traditional hydrology-based method, employs slope data interpreted from a digital elevation model (DEM) to segment more suitable slope units. This method takes into account the influence of topographic relief and better reduces the interference in the segmentation results[28]. In addition, the approach can provide more uniform units and increase slope unit partition precision[11], [29].

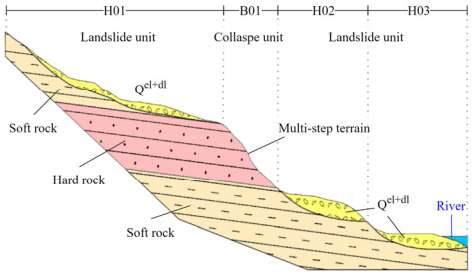


**Figure 3.** Schematic diagram of the multi-scale division of slope units

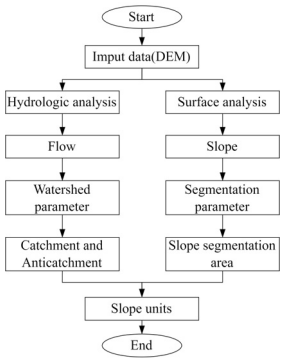


**Figure 4.** The hydrology-based and slope segmentation method of extraction of slope units

### 2.4 Hazard Evaluation Methods

Hazard evaluation is a fundamental step in reducing the risk of geological disaster, which needs to consider the uncertainty characteristics of triggering factors, such as rainfall, reservoir water, and earthquake[30]. To calculate the rainfall conditions for different return periods, a rainfall probability distribution model has been established, which can be combined with the limit equilibrium analysis method for slope stability evaluation[31]. The evaluation process is to use the Slope module of Geo-studio software[32]. The slope engineering geological profile is regarded as the calculation profile. Also, different return periods of rainfall conditions are considered. Subsequently, the Bishop method is selected to numerically simulate each slope unit[33]. Then, the instability probability is determined according to the Monte-Carlo simulation, where the slope stability coefficient and instability probability under different rainfall conditions can be obtained.

#### 2.4.1 Rainfall Frequency Analysis

The meteorological rainfall data follows an exponential asymptotic distribution, i.e., the Gumbel distribution. This probability density function is defined by:

$$F(x) = P(\xi < x) = e^{-e^{-a(x-u)}} \tag{1}$$

where $a$ is location parameter, $u$ is scale parameter and $x$ denotes the random variable.

The rainfall intensity $R_T$ for a certain recurrence period $T$ is given by

$$R_T = u - \frac{1}{a}[\ln(\ln\frac{T}{T-1})] \tag{2}$$

#### 2.4.2Bishop's Modified Method

The Bishop method is widely used for the stability calculation of gravel soil landslides[34]. It is assumed that the slip crack surface is circular, and the combined forces act horizontally between the soil bars. Then the moment balance condition can be applied to obtain the solution.

$$N_1 = W\sin a \tag{3}$$

$$N_2 = \frac{[\frac{W}{\cos a} - ul]\tan\phi + cl}{1 + \frac{\tan a\tan\phi}{F_a}} \tag{4}$$

$$F_c = \frac{\sum N_2}{\sum N_1} \tag{5}$$

where $W$ is the weight of slice, $c$ is cohesion intercept, $\phi$ is friction angle, $u$ is pore pressure, $a$ is the angle between the base of slice and horizontal, and $l$ is the length of slip surface segments measured along the base of the slice. $F_a$ is an assumed $F$, and $F_c$ means the calculated $F$.

### 2.4.3 Rigid Body Limit Equilibrium Method

The rigid body limit equilibrium method is one of the traditional methods for stability analysis, its effectiveness is confirmed by factual engineering[35]. The safety coefficient is always used to judge the dangerous rock mass safety degree. The stability coefficient of the dangerous rock mass is calculated by Eq. (6).

$$F = \frac{(W\cos\theta - Q\sin\theta - V\sin\theta - V)\tan\phi + cl}{W\sin\theta + Q\cos\theta + V\cos\theta} \tag{6}$$

where $F$ is the stability factor, $W$ is the weight of rock, $\theta$ is inclination of soft structural surface, $Q$ is torque of earthquake, $V$ is fracture water pressure, $c$ is a cohesion coefficient, $l$ is the length of the sliding surface, and $\phi$ is the angle of internal friction.

## 2.5 Vulnerability Evaluation Methods

Vulnerability refers to the degree of destruction or damage that occurs to one or more affected objects under a specific geohazard intensity[36]. Vulnerability indicates the degree of interaction between the geohazard intensity and the disaster-bearing body. Therefore, evaluation of vulnerability can help to reduce the risk of geological disaster[37], [38].

Vulnerability refers to the degree of destruction or damage that occurs to one or more affected objects under a specific geohazard intensity[36]. Thus, vulnerability evaluation can help to quantify the relationship between geological disasters and the hazard-bearing body.

### 2.5.1 Object-Oriented Disaster-Bearing Body Extraction Method

UAV remote sensing imagery has a high resolution that contains a large amount of feature information, but it also raises challenges for data processing. Traditional pixel-based classification methods produce salt and pepper noise, causing a low classification accuracy. Therefore, object-oriented classification methods are adopted, which can take into account the spectral , texture, and context information , with a high accuracy of the classification. [39] Image segmentation plays an important role in object-oriented classification methods and directly affects the accuracy of the classification results. It employs the Estimation of Scale Parameters (ESP) tool to calculate the optimal segmentation scale. The tool selected two parameters, local variance, and rate of change, to evaluate the multi-scale segmentation results. The higher of the local variance means the more delicate of the segmentation result, and the greater complexity of the classification. The rate of change is the speed at which the information on the segmentation results changes between the two scales. The process of object-oriented multi-scale segmentation is shown in Figure 5. The first step of the extraction is to determine the optimal image segmentation scale through large range pre-segmentation, small range step-by-step segmentation, and scale parameter evaluation. Then, the typical disaster-bearing bodies are selected to build the classification training samples, which will be used to classify the image segmentation objects according to the spectral factors and shape factors. Finally, the images are classified into four categories, including buildings, roads, fruit forests, and fish ponds.

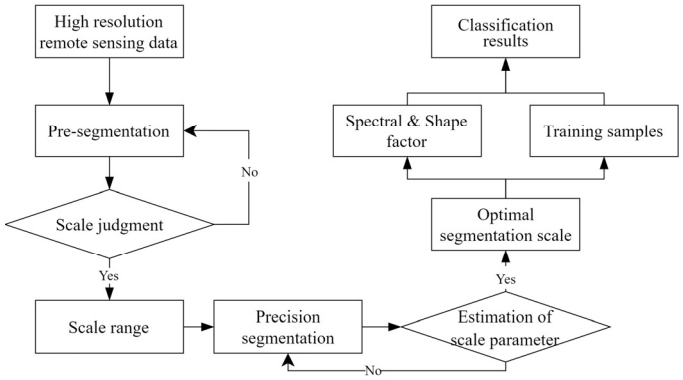


**Figure 5.** An object-oriented automatic extraction method for the disaster-bearing body

### 2.5.2Quantitative Calculation Method of Vulnerability

As mentioned above, vulnerability is a function of the intensity of the hazard and the resilience of the disaster-bearing body. The intensity of the hazard is inversely proportional to the landslide run-out distance or rockfall travel distance. The resilience of the disaster-bearing body is related to its structural type and construction materials. To facilitate comparative calculations, the intensity of the hazard and the resilience of the disaster-bearing body were normalized. Then, the empirical model proposed by Li [40] was adopted for geological disaster susceptibility evaluation, as shown in Eq. (7).

$$V = f(I,R) = \begin{cases} \dfrac{2I^2}{R^2} & \dfrac{I}{R} \le 0.5 \\ 1.0 - \dfrac{2(R-I)^2}{R^2} & 0.5 < \dfrac{I}{R} \le 1.0 \\ 1.0 & \dfrac{I}{R} > 1.0 \end{cases} \tag{7}$$

where $V$ denotes vulnerability factor, $I$ is the intensity of the hazard, and $R$ is the resilience of the disaster-bearing body.

## 3 Results & Discussion

### 3.1 Division Of Slope Evaluation Units

The study area was divided into seven slope units as shown in Figure 6a using traditional hydrological analysis for slope unit division. While using the improved slope splitting method for secondary division of slope units, the study area was divided into 20 slope units, including 14 landslide assessment units and 6 collapse assessment units, as shown in Figure 6b. By comparing the slope unit division results, the improved slope splitting method performs better not only on

spatial segmentation, but also on slope type determination, such as landslide or collapse, than the traditional hydrological analysis method.

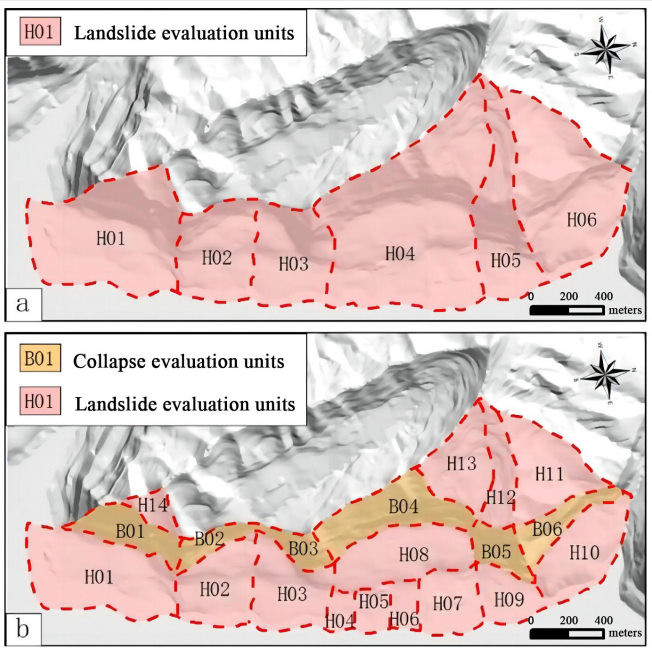


**Figure 6.** Maps of slope units extracted by two methods, (a) traditional hydrology-based method (b) slope segmentation method.

### 3.2 Extraction Of Disaster-Bearing Bodies

Using UAV remote sensing images with a resolution of 0.1m as the data source, the results of the ESP estimation based on the multi-scale segmentation method are shown in Figure 7. The segmentation scale varies from 100 to 1100. As the segmentation scale increases, the local variance of the segmentation results tends to increase. When the segmentation scale is 260, the rate of change is zero at first time. Considering the delicacy of the segmentation and the complexity of the classification, the optimal segmentation scale is 260. By selecting training samples of classification objects, image classification was done with the nearest neighbor method and then categorized into 4 types, including building, road, fruit forest, and fish pond according to reality, as shown in Figure 8. The number of the extracted buildings is 600 and the area is 93.8 $\times 10^3$ m$^2$. The length of the extracted road is 14,400 meters and the area is 89.3 $\times 10^3$ m$^2$. The area of fruit forest is 1985.2$\times 10^3$ m$^2$. The area of fish pond is 40.1$\times 10^3$ m$^2$. In terms of area, fruit forests occupy the majority of the study area. However, in terms of socio-economic value, buildings and roads are the main disaster-bearing bodies.

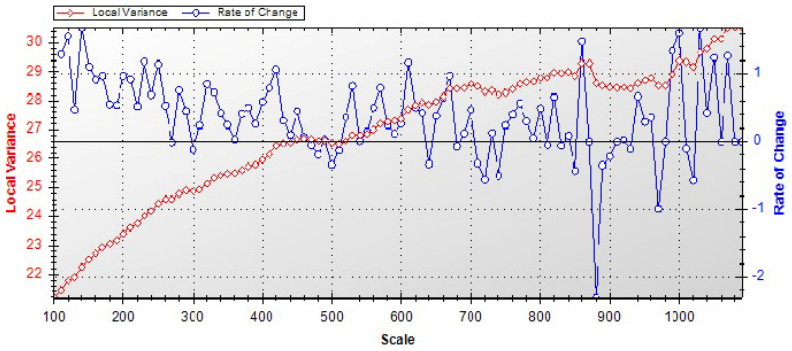


**Figure 7.** Estimation of Scale Parameters (ESP)

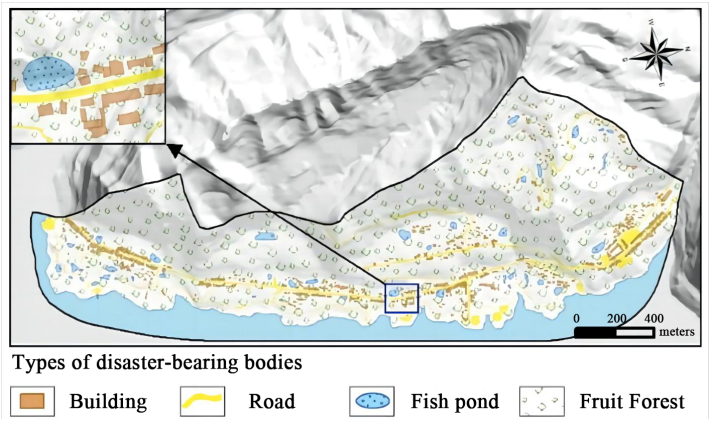


**Figure 8.** Extraction result map of the disaster-bearing body

### 3.3 Evaluation Of Geological Disaster Risk

A complete geological disaster risk evaluation incorporates two assessment phases: the hazard and the vulnerability[41]. The hazard evaluation results indicated that under the 50-year rainfall condition (i.e., rainfall probability = 2%), there were 6 very high hazard slope units (i.e., 4 landslide units and 2 collapse units), 5 high hazard slope units (i.e., 4 landslide units and 1 collapse unit), 4 medium hazard areas (i.e., 4 landslide units), and 5 low hazard slope units (i.e., 2 landslide units and 3 collapse units), as shown in Figure 9a.

The vulnerability evaluation was to calculate the intensity of hazard and the resistance of the disaster-bearing body quantitatively by Eq. (7) and classify the results into different classes, i.e., very high (0~0.3), high (0.3~0.5), medium (0.5~0.7), low (0.7~0.9). The results indicated that about $5.4\times10^3$ $m^2$ of buildings and $3.4\times10^3$ $m^2$ of roads were in the very high vulnerability zone, about $51.5\times10^3$ $m^2$ of buildings and $11.4\times10^3$ $m^2$ of roads were in the high vulnerability zone, about $18.3\times10^3$ $m^2$ of buildings and $52.8\times10^3$ $m^2$ of roads were in the medium vulnerability zone, about $18.6\times10^3$ $m^2$ of buildings and $21.7\times10^3$ $m^2$ of roads were in the low vulnerability zone, as shown in Table 2 and Figure 9b.

The geological disaster risk level map is the final product of geological disaster risk evaluation. Based on hazard and vulnerability, geological disaster risk evaluation adopts the matrix criterion method to realize the risk level classification. The results indicated that about $34.5\times10^3$ $m^2$ of buildings and $15.0\times10^3$ $m^2$ of roads were in the very high risk zone, about $36.3\times10^3$ $m^2$ of buildings and $38.3\times10^3$ $m^2$ of roads were in the high risk zone, about $4.4\times10^3$ $m^2$ of buildings and $17.5\times10^3$ $m^2$ of roads were in the medium risk zone, about $18.6\times10^3$ $m^2$ of buildings and $18.5\times10^3$ $m^2$ of roads were in the low risk zone, as shown in Table 3 and Figure 9c.

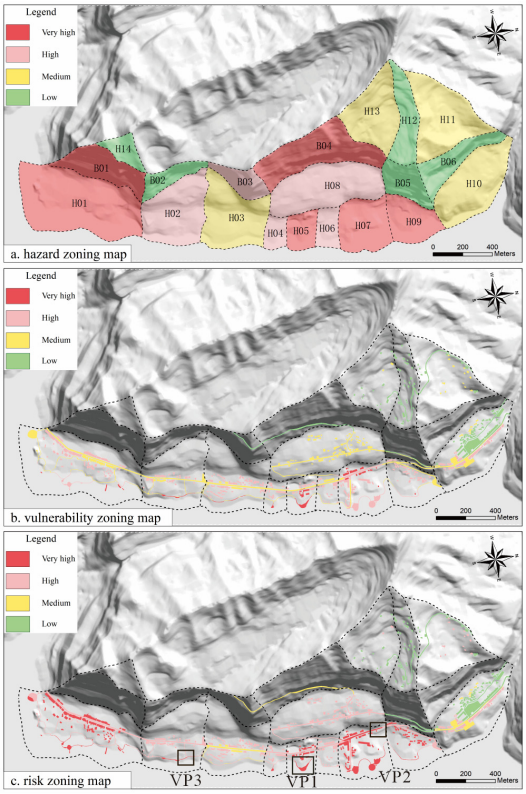


**Figure 9.** A series of maps for geological disaster risk evaluation in town, (a) hazard zoning map, (b) vulnerability zoning map, (c) risk zoning map.

**Table 2** Vulnerability evaluation of Dazhou town

| Level | Building | | Road | |
|---|---|---|---|---|
| | *Area ($10^3m^2$)* | *Percentage* | *Area ($10^3m^2$)* | *Percentage* |
| Very high | 5.4 | 5.76% | 3.4 | 3.81% |
| High | 51.5 | 54.90% | 11.4 | 12.77% |
| Medium | 18.3 | 19.51% | 52.8 | 59.13% |
| Low | 18.6 | 19.83% | 21.7 | 24.30% |

**Table 3** Risk evaluation of Dazhou town

| Level | Building | | Road | |
|---|---|---|---|---|
| | *Area ($10^3m^2$)* | *Percentage* | *Area ($10^3m^2$)* | *Percentage* |
| Very high | 34.5 | 36.78% | 15.0 | 16.80% |
| High | 36.3 | 38.70% | 38.3 | 42.89% |
| Medium | 4.4 | 4.69% | 17.5 | 19.60% |
| Low | 18.6 | 19.83% | 18.5 | 20.72% |

Three sites were selected from the very highly risky zone for validation purposes. According to the field survey and monitoring information, a comprehensive assessment of the chosen sites was made, as shown in Figure 9c and Figure 10. Verification point No. 1 (VP1) is a viewing platform along the Yangtze River, where the slope is under continuous slow deformation with a maximum crack of 10cm, and the monitoring data showed a deformation rate of 4cm/year. The verification point is a tourist hotspot of the town. Thus, we comprehensively assessed the risk level to be very high. Verification point No.2 (VP2) is located at the back edge of the Qingkangling landslide. Through field investigation, we found that the landslide is in deformation state, resulting in house cracking up to 5cm, threatening 5 people, and causing a potential economic loss of 0.3 million RMB. Therefore, the risk level of this verification point is assessed to be very high. Verification point No. 3 (VP3) is located in the protective engineering zone along the river. Affected by the fluctuations of the reservoir water level, the slope deformation is significant, and the maximum deformation drop is 3.5 meters. The annual deformation amount is 10~15cm/year. The disaster-bearing body is the viewing trail and cottages, and the potential economic loss is about 2 million RMB. Therefore, the comprehensive evaluation of this point has a high risk. The verification results show that the geological disaster risk evaluation results are consistent with the field survey and monitoring, indicating that the evaluation results are accurate and reliable.

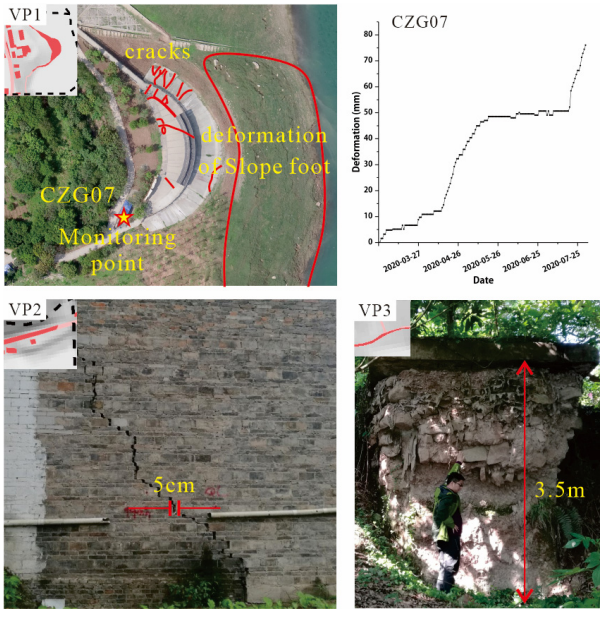


**Figure 10.** Results of the validation of the geological disaster risk evaluation.

## 4 Conclusions

This paper proposes a technical method for town scale geological disaster risk evaluation. By focusing on improving and optimizing the division of slope units and extraction of disaster-bearing bodies, the proposed method shows superior performance to the traditional method in terms of accuracy and effectiveness of risk evaluation.

Taking Dazhou town as an example, we evaluated the risk level of geological disasters under 50-year rainfall return period conditions and achieved reasonable and reliable evaluation results that were in line with the actual situation, which could provide reference for the risk evaluation of geological disaster in towns along the Three Gorges Reservoir area.

Accurate and dynamic evaluation and application of geologic disaster risk will be the future trend, which will play an important role for local geohazard prevention and control as well as a territory development plan.

**Acknowledgment:** The authors are grateful to the financial supports from National Key R&D Program of China (Grant No. 2019YFC1509605), the Open Project Program of Hebei Center for Ecological and Environmental Geology Research (No.JSYF-202203), and Geological Survey Project (Grant No. DD20221813).

## References

[1] Y. Yin, "Human-cutting slope structure and failure pattern at the three gorges reservoir.," *Journal of Engineering Geology*, vol. 13, no. 2, pp. 145–154, Apr. 2005.

[2] Yueping Yin *et al.*, "Reservoir-induced landslides and risk control in Three Gorges Project on Yangtze River, China," *Journal of Rock Mechanics and Geotechnical Engineering*, vol. 8, no. 5, pp. 577–595, Oct. 2016.

[3] Huiming Tang, Janusz Wasowski, and C. Hsein Juang, "Geohazards in the three Gorges Reservoir Area, China – Lessons learned from decades of research," *Engineering Geology*, vol. 261, p. 105267, Nov. 2019, doi: 10.1016/j.enggeo.2019.105267.

[4] B. Huang, Y. Yin, B. Li, W. Feng, Z. Qin, and P. Zhang, "Study of risk assessment and mitigation for landslide-induced impulse wave near towns in reservoir areas," Acta Geologica Sinica, vol. 95, no. 06, pp. 1949–1961, 2021.

[5] C. W. W. Ng, B. Yang, Z. Q. Liu, J. S. H. Kwan, and L. Chen, "Spatiotemporal modelling of rainfall-induced landslides using machine learning," *Landslides*, vol. 18, no. 7, pp. 2499–2514, Jul. 2021.

[6] Ling Peng, Suning Xu, Jinwu Hou, and Junhuan Peng, "Quantitative risk analysis for landslides: the case of the Three Gorges area, China," *Landslides*, vol. 12, no. 5, pp. 943–960, Oct. 2015.

[7] Lili Xiao, Jiajia Wang, Yanbo Zhu, and Jun Zhang, "Quantitative Risk Analysis of a Rainfall-Induced Complex Landslide in Wanzhou County, Three Gorges Reservoir, China," *Int J Disaster Risk Sci*, vol. 11, no. 3, pp. 347–363, Jun. 2020.

[8] F. Wang, K. Yin, L. Gui, and L. Chen, "Risk Analysis on Individual Reservoir Bank Landslide and Its Generated Wave," Earth Science, vol. 43, no. 03, pp. 899–909, 2018.

[9] Zhice Fang, Yi Wang, Ling Peng, and Haoyuan Hong, “A comparative study of heterogeneous ensemble-learning techniques for landslide susceptibility mapping,” *International Journal of Geographical Information Science*, vol. 35, no. 2, pp. 321–347, Feb. 2021.
[10] Chiranjib Prasad Sarma, Arindam Dey, and A. Murali Krishna, “Influence of digital elevation models on the simulation of rainfall-induced landslides in the hillslopes of Guwahati, India,” *Engineering Geology*, vol. 268, p. 105523, Apr. 2020.
[11] Faming Huang *et al.*, “Efficient and automatic extraction of slope units based on multi-scale segmentation method for landslide assessments,” *Landslides*, Sep. 2021.
[12] Qulin Tan, Yong Huang, Jun Hu, Pinggen Zhou, and Jiping Hu, “Application of artificial neural network model based on GIS in geological hazard zoning,” *Neural Comput & Applic*, vol. 33, no. 2, pp. 591–602, Jan. 2021.
[13] Wengang Zhang, Hongrui Li, Liang Han, Longlong Chen, and Lin Wang, “Slope stability prediction using ensemble learning techniques: A case study in Yunyang County, Chongqing, China,” *Journal of Rock Mechanics and Geotechnical Engineering*, 2022.
[14] Yu Zhao, Rui Wang, Yuanjun Jiang, Huajun Liu, and Zhenlei Wei, “GIS-based logistic regression for rainfall-induced landslide susceptibility mapping under different grid sizes in Yueqing, Southeastern China,” *Engineering Geology*, vol. 259, p. 105147, Sep. 2019.
[15] Liang Lv, Tao Chen, Jie Dou, and Antonio Plaza, “A hybrid ensemble-based deep-learning framework for landslide susceptibility mapping,” *International Journal of Applied Earth Observation and Geoinformation*, vol. 108, p. 102713, Apr. 2022.
[16] Abhirup Dikshit, Neelima Satyam, Biswajeet Pradhan, and Sai Kushal, “Estimating rainfall threshold and temporal probability for landslide occurrences in Darjeeling Himalayas,” *Geosci J*, vol. 24, no. 2, pp. 225–233, 2020.
[17] Chuanming Ma, Zhiwei Yan, Peng Huang, and Lin Gao, “Evaluation of landslide susceptibility based on the occurrence mechanism of landslide: a case study in Yuan’ an county, China,” *Environ Earth Sci*, vol. 80, no. 3, p. 94, Jan. 2021.
[18] F. Huang, Z. Cao, C. Yao, Q. Jiang, and J. Chen, “Landslides hazard warning based on decision tree and effective rainfall intensity,” Journal of ZheJiang University (Engineering Science), vol. 55, no. 03, pp. 472–482, 2021.
[19] Y. Liu, Z. Zhang, and Y. Su, “Case study of vulnerability evaluation geo-hazards bearing capacity of a region,” Journal of Engineering Geology, vol. 26, no. 05, pp. 1121–1130, 2018.
[20] Shuai Zhang, Can Li, Limin Zhang, Ming Peng, Liangtong Zhan, and Qiang Xu, “Quantification of human vulnerability to earthquake-induced landslides using Bayesian network,” *Engineering Geology*, vol. 265, p. 105436, Feb. 2020, doi: 10.1016/j.enggeo.2019.105436.
[21] Settimio Ferlisi, Giovanni Gullà, Gianfranco Nicodemo, and Dario Peduto, “A multi-scale methodological approach for slow-moving landslide risk mitigation in urban areas, southern Italy,” *Euro-Mediterr J Environ Integr*, vol. 4, no. 1, p. 20, 2019.
[22] H. Lan, N. Zhang, and L. Li., “Risk analysis of major engineering geological hazards for Sichuan-Tibet Railway in the phase of feasibility study,” Journal of Engineering Geology, vol. 29, no. 02, pp. 326–341, 2021.
[23] M. Zhang, Q. Xue, J. Jia, J. Xu, B. Gao, and J. Wang, “Methods and Practices for the Investigation and Risk Assessment of Geo-hazards in Mountainous Towns,” Northwestern Geology, vol. 52, no. 02, pp. 125–135, 2019.
[24] S. Wu, J. Shi, T. Wang, C. Zhang, and L. Shi, Theory and Techniques of Landslide Risk Assessment, 1rd ed., Beijing: Science Press, 2012, pp.79–81.

[25] W. Huabin, L. Gangjun, X. Weiya, and W. Gonghui, “GIS-based landslide hazard assessment: an overview,” *Progress in Physical Geography: Earth and Environment*, vol. 29, no. 4, pp. 548–567, Dec. 2005.
[26] X. Yang et al., “Progress of geological hazards survey in the urban area from Wanzhou to Wushan in Three Gorges Reservoir,” Geological Survey of China, vol. 8, no. 01, pp. 97–107, 2021.
[27] W. WU, F REN, R NIU, and L PENG, “Landslide Spatial Prediction Based on Slope Units and Support Vector Machines,” Geomatics and Information Science of Wuhan University, vol. 38, no. 12, pp. 1499–1503, 2013.
[28] Zhuo Chen, Shouyun Liang, Yutian Ke, Zhikun Yang, and Hongliang Zhao, “Landslide susceptibility assessment using different slope units based on the evidential belief function model,” *Geocarto International*, vol. 35, no. 15, pp. 1641–1664, Nov. 2020
[29] Yange Li, Guangqi Chen, Bo Wang, Lu Zheng, Yingbin Zhang, and Chuan Tang, “A new approach of combining aerial photography with satellite imagery for landslide detection,” *Nat Hazards*, vol. 66, no. 2, pp. 649–669, Mar. 2013
[30] D. Jimenez-Peralvarez, R. El Hamdouni, J. A. Palenzuela, C. Irigaray, and J. Chacon, “Landslide-hazard mapping through multi-technique activity assessment: an example from the Betic Cordillera (southern Spain),” *Landslides*, vol. 14, no. 6, pp. 1975–1991, Dec. 2017.
[31] Arash Hassanikhah and Eric C. Drumm, “Stability and Evolution of Planar and Concave Slopes under Unsaturated and Rainfall Conditions,” *International Journal of Geomechanics*, vol. 20, no. 7, 2020.
[32] Lin Wang, Chongzhi Wu, Yongqin Li, Hanlong Liu, Wengang Zhang, and Xiang Chen, “Probabilistic Risk Assessment of unsaturated Slope Failure Considering Spatial Variability of Hydraulic Parameters,” *Ksce Journal of Civil Engineering*, vol. 23, no. 12, pp. 5032–5040, Dec. 2019.
[33] Tianfeng Gu, Jiading Wang, and Xinping Fu, “Regional Slope Stability Analysis Method Based on the Slope Unit,” *Scientia Geographica Sinica*, vol. 33, no. 11, pp. 1400–1405, 2013.
[34] Dong Tang, Zhongming Jiang, Tao Yuan, and Yi Li, “Stability Analysis of Soil Slope Subjected to Perched Water Condition,” *KSCE Journal of Civil Engineering*, vol. 24, no. 9, 2020.
[35] Nikhil Kumar, A. K. Verma, Sahil Sardana, K. Sarkar, and T. N. Singh, “Comparative analysis of limit equilibrium and numerical methods for prediction of a landslide,” *Bulletin of Engineering Geology and the Environment*, vol. 77, no. 2, pp. 595–608, May 2018.
[36] Q. Chen *et al.*, “Assessment of the physical vulnerability of buildings affected by slow-moving landslides,” *Natural Hazards and Earth System Sciences*, vol. 20, no. 9, pp. 2547–2565, Sep. 2020.
[37] H. E. Martinez Carvajal, M. T. de M. Guimaraes Silva, E. F. Garcia Aristizabal, E. V. Aristizabal-Giraldo, and M. A. Larios Benavides, “A mathematical approach for assessing landslide vulnerability,” *Earth Sciences Research Journal*, vol. 22, no. 4, pp. 251–273, Oct. 2018.
[38] A. Singh, D. P. Kanungo, and S. Pal, “Physical vulnerability assessment of buildings exposed to landslides in India,” *Natural Hazards*, vol. 96, no. 2, pp. 753–790, Mar. 2019.
[39] Tianbo Chen, Zhuowei Hu, Lai Wei, and Shunqiang Hu, “Data Processing and Landslide Information Extraction Based on UAV Remote Sensing,” *Journal of Geo-Information Science*, vol. 19, no. 5, pp. 692–701, 2017.
[40] Zhihong Li, Farrokh Nadim, Hongwei Huang, Marco Uzielli, and Suzanne Lacasse, “Quantitative vulnerability estimation for scenario-based landslide hazards,” *Landslides*, vol. 7, no. 2, pp. 125–134, Jun. 2010.
[41] M. Michael-Leiba, F. Baynes, G. Scott, and K. Granger, “Regional landslide risk to the Cairns community,” *Natural Hazards*, vol. 30, no. 2, pp. 233–249, Oct. 2003.